2025-24-0009 Published 07 Sep 2025

CFD Simulation of Combustion in an Optically Accessible Hydrogen Engine: Comparison between Lean and Diluted Stoichiometric Operations

Manuel Madia Universita di Modena e Reggio Emilia

Benjamin Boehm TU Darmstadt

Stefano Fontanesi Universita di Modena e Reggio Emilia

Pedro Ye TU Darmstadt

Mauro Magnani and Sebastiano Breda Universita di Modena e Reggio Emilia

Citation: Madia, M., Boehm, B., Fontanesi, S., Ye, P. et al., "CFD Simulation of Combustion in an Optically Accessible Hydrogen Engine: Comparison between Lean and Diluted Stoichiometric Operations," SAE Technical Paper 2025-24-0009, 2025, doi:10.4271/2025-24-0009.

Received: 05 May 2025 Revised: 27 Jun 2025 Accepted: 27 Jun 2025

Abstract

The reduction of CO2 emissions from anthropogenic activities is pushing the green energy transition, prompting the search for alternative and more environmental-friendly solutions compared to traditional technologies based on fossil fuels. One of the most affected sectors is transportation, which is undergoing a significant change to increase sustainability. To achieve this goal, development of hybrid and electric propulsion systems has taken hold over the past decade, but electrification is proceeding slower than expected due to many challenges related to charging infrastructure, cars range and cost, thus pushing the European automotive sector into a potential crisis. To reverse this trend and simultaneously accelerate the transition to sustainable transportation, further development of ICEs technology aimed at enhancing efficiency when using alternative fuels like hydrogen, is staging a comeback. Thanks to the possibility to retrofit existing units, benefiting from a strong know-how and a developed supply chain, hydrogen fuelled ICEs are an attractive mid-term solution. The application of reliable numerical models can support the retrofitting, providing a deep insight into in-cylinder processes such as injection and combustion, enabling virtual optimizations and reducing development costs and time to market. Comprehensive experimental campaigns on research engines are necessary to develop and validate advanced numerical models, identifying potential weaknesses in the modelling approach. In the current work, experimental results on the Darmstadt optical-accessible engine are applied to validate a 3D CFD framework for the simulation of hydrogen combustion in ultra-lean and stoichiometric ultra-diluted conditions. A detailed analysis of the experienced combustion regime is provided to address the validity of the adopted modelling assumptions as well as the possible occurrence of flame instabilities. This lays the foundation for future model development. The modelling of quenching and a detailed representation of piston crevices contribute to improved accuracy in both operating conditions.

Introduction

The increasing concern over climate change has pushed European Union to implement further stringent regulations to limit the greenhouse gases emissions. Indeed, a target of a 55% reduction of the global CO2 emitted is set for 2030, while the complete carbon neutrality is expected to be matched in 2050 [1]. In this scenario, hydrogen-fuelled internal combustion engines (H_2ICEs) can be an additional tool that can be used to decarbonize the transport sector, together with Battery Electric Vehicles (BEVs) and Fuel Cell Electric Vehicles (FCEVs). Indeed, this solution would take advantage of the extended expertise of the manufacturers concerning the internal combustion engine technology, and thus reducing the overall time needed for the transition to a cleaner mobility, while exploiting the zero-carbon

footprint of hydrogen combustion [2]. However, there are several characteristics of hydrogen that make its adoption as a fuel challenging. For instance, its low density limits the trapping efficiency and trapped energy in the combustion chamber, and thus the power output, when a Port Fuel Injection (PFI) architecture is adopted. Despite Direct Injection (DI) can thoroughly avoid this problem, its implementation is less straightforward, with a higher cost due to the high-pressure injection system. Moreover, the DI solution needs to be accurately studied and optimised, as the injection strategy strongly affects the mixture formation, and thus the combustion development and the pollutant emissions [3, 4, 5, 6]. In addition, hydrogen's low quenching distance may affect the near-wall flame behaviour, increasing the heat transferred to the walls with respect to a fossil fuel for a given energy content in the combustion chamber. Besides, the tendency to experience abnormal combustion events, such as pre-ignition, auto-ignition and surface ignition, needs to be carefully addressed and, if needed, the engine system must be modified. For instance, to avoid wide zones with a high surface-to-volume ratio, which can unwillingly trigger ignition by a hotspot, the geometrical characteristics of the combustion chamber may be modified. In addition, alternative strategies to lower the knock and pre-ignition tendency of a hydrogen mixture in both PFI and DI can be implemented, such as cooling the mixture before entering the combustion chamber [7, 8], advancing hydrogen's start of injection [9] or considering water injection [10]. Despite these challenges, hydrogen has plenty of characteristics which make it a viable fuel to be used in ICEs. First of all, the high laminar flame speed values, higher than the traditional fuels over a wide range of equivalence ratios (Φ), allows a fast combustion rate, and thus a high thermal efficiency. Secondly, the high lower heating value, approximately three times higher than its carbon-based counterpart, makes the mass-based energy content of a hydrogen mixture comparable to a gasoline one for a given Φ, despite its high stoichiometric air-to-fuel ratio and its low density, which can affect the trapped energy in the combustion chamber [8, 11]. Thirdly, hydrogen is characterized by a wide flammability range, spanning from Φ = 0.1 to 7.1 [12, 13], which allows the H_2ICE operating load to be controlled directly through the mixture quality rather than a throttled valve, thus reducing the pumping losses [14].

Given these characteristics, the optimal operating condition of a H_2ICE cannot be defined a priori and has to be carefully studied. Hence, the combination of experimental and numerical investigations can accelerate the learning process of all the phenomena which take place in the combustion chamber, and 3D CFD numerical simulations can play a key role in this scenario. For instance, Rakopoulos et al. [15] adopted an in-house CFD code to characterized hydrogen combustion in a Cooperative Fuel Research (CFR) engine with three different lean mixtures, with a good agreement with experimental data. Sfriso et al. [16] proposed a CFD framework to accurately predict hydrogen lean combustion in a DI engine, retrofitted from a diesel one, in a wide range of Φ and engine speeds, and a well-matched numerical-experimental comparison was found. Additionally, the same authors also proved that the proposed methodology is able to predict the NO_x emissions [17]. Dyhani et al. [18] detected experimentally the backfiring tendency of a PFI hydrogen engine, and CFD simulations were adopted to characterize the backfire onset in terms of timing, magnitude, and dependency on the hotspot temperature and location.

The engine analysed in this work, which will be further described in the next section, is an optically-accessible unit with a PFI architecture. Several works can be found in literature concerning the numerical-experimental comparison considering the same engine. Iacovano et al. [19] numerically investigated the engine motored condition through 1D and 3D CFD simulations, studying the impact on the results of the crevice geometry, along with the modeling of blow-by and heat transfer. Raj et al. [20] analysed the coldflow phase of the same engine with CFD in RANS framework, and they examined the impact of two different turbulence models on the in-cylinder pressure profile, comparing it with the experimental data. Barbato et al. [21] considered the same experimental basis to numerically investigate the motored condition with CFD in both RANS and LES frameworks, and a study on the impact of several mesh setups on the result has been conducted.

The aim of this study is the understanding of hydrogen combustion in an internal combustion engine at two operating conditions showing similar IMEPs but different strategies, exploiting hydrogen's wide flammability limits. For instance, while both run with the same engine speed and intake pressure, the first operating condition is fuelled with a lean mixture, with an air-to-fuel ratio (λ) of 2.53, while the second one considers a stoichiometric mixture with a EGR dilution of 40%.

Experimental Setup and Analysed Cases

The experiments were performed in the Darmstadt engine. It is a four-stroke, single-cylinder, spark-ignited optically accessible engine. It has a compression ratio of 8.7; bore and a stroke of 86 mm; a spray-guided, 4-valve pent-roof cylinder head geometry; centrally mounted spark plug; and a flat piston surface. In order to avoid damaging the optical liner, the piston rings are located 74 mm from the piston top, contributing to a larger than usual crevice volume of typical engines. More details of the engine setup are shown in Figure 1 and can be found in [22, 23].

Operating conditions are summarized in Table 1. The fuel was injected 540 mm upstream of the intake valves, ensuring a homogeneous air-fuel mixture in the cylinder. The ignition timings (t_{ign}) were chosen in order to obtain similar MFB50 between both operating conditions (OC). A gas mixture system mixed dry air with pure nitrogen in the desirable amount upstream of a storage plenum.

FIGURE 1 Experimental setup schematic.

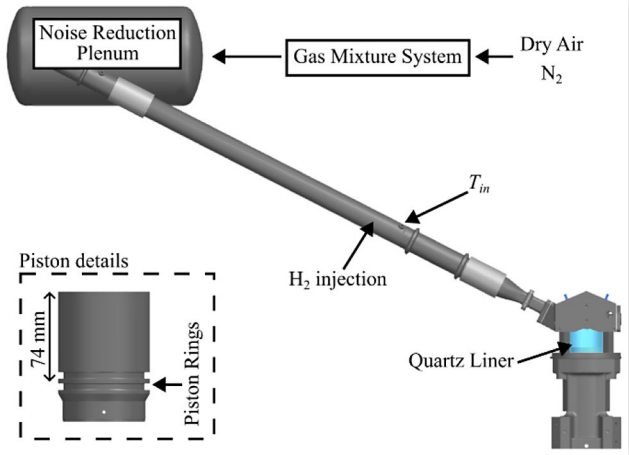

TABLE 1 Operating conditions studied. Spark timing is expressed in crank angle degrees after compression top dead centre.

OC	Lean	Diluted
N (rpm)	800	800
p_{in} (bar)	0.95	0.95
t_{ign} (CAD aTDC)	-16.6	-8.8
λ (-)	2.53	1
N_2 volume fraction (%)	0	40
T_{in} (K)	304	308

The mixture was led to a noise reduction plenum before entering the intake manifold and its temperature (T_{in}) was probed 480 mm upstream of the intake valves.

Numerical Setup

In this section, the setup adopted in the numerical simulations is briefly reported. The simulations are performed in a RANS framework using Star-CCM+ v2024.02, a commercial 3D-CFD software licensed by Siemens DISW. To manage the motion of engine components, the in-Cylinder tool is used.

As for the turbulence modelling, the $k-\varepsilon$ RNG turbulence model [24] is selected. A two-Layer All y+ wall treatment is used with two prismatic layer on the solid surfaces, each one 0.375 mm thick. The GruMo-UniMORE Wall Heat Transfer Model [25, 26, 27] is employed.

The cell size in the combustion chamber is fixed at 0.75 mm, with two additional refinements around the spark plug during the combustion phase to gradually reduce the cell size down to 0.1875 mm near the spark electrodes, while in the ports the maximum cell size is fixed at 3.0 mm. The timestep ranges from 0.0125 crank angle degrees (CAD) at opening/closing valve events to 0.05 CAD during the compression and exhaust stroke. During the early flame kernel development, the timestep is set to 0.01 CAD. This setup leads to a computational

FIGURE 2 Spark plug electrical circuit.

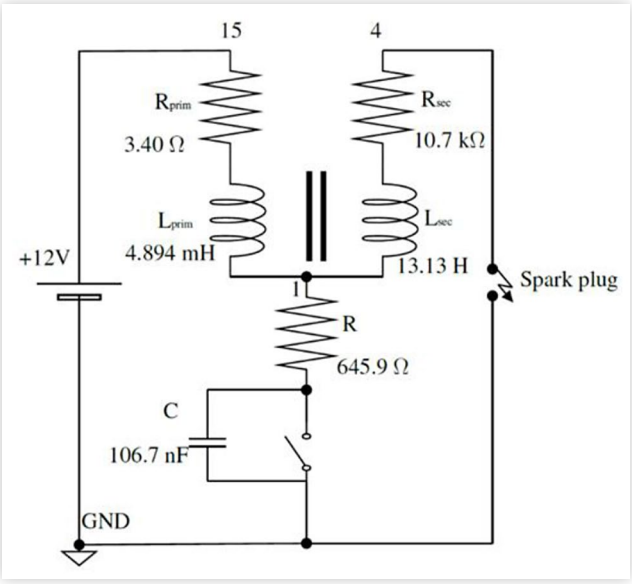

grid of nearly 3 million cells at BDC and 2.1 million cells at TDC, with a cumulative elapsed time of 30 hours on 104 cores for a full cycle simulation. Two consecutive cycles are executed to get rid of the influence of initial conditions and reach cyclic convergence. The pressure traces at the inlet and outlet boundaries come from experiments, even if the pressure outlet sensor is pegged to match the trapped mass calculated from the measured mass flow rate. Concerning the temperature at the inlet boundary, it is set constant and equal at the average temperature measured all over the experimental cycles acquired.

The ISSIM spark-ignition model [28, 29] is used at electrical spark time to initialize the combustion process, considering the spark-plug electrical circuit depicted in Figure 2. To simulate the combustion process the turbulent flame closure (TFC) model is used considering a chemical equilibrium with a single step reaction. The laminar flame speed is imposed using the Verhelst correlation [30] based on the Konnov 1D chemical mechanism [31] for hydrogen oxidation without considering flame instabilities. This correlation is well validated for the ranges of interest of each of pressure, temperature, equivalence ratio and EGR ($5 \le p$ [bar] ≤ 45, $500 \le T$ [K] ≤ 900, $0.2 \le \Phi \le 3$, $0 \le$ EGR [%mol] ≤ 50).

$$S_T = S_L \left[1 + A \cdot \left(\frac{u'}{S_L} \right)^{5/6} \right] \tag{1}$$

$$l_q = 5 \cdot \left(11.5 \cdot \frac{\mu}{c_\mu^{0.25} \rho k^{0.5}} \right) \tag{2}$$

The turbulence flame closure is provided through the Damköhler correlation reported in Equation 1, where S_L is the laminar flame speed, A is an empirical coefficient set equal to 3.0 and u' is the turbulent fluctuation.

Such approach has proven to be able to correctly estimate the hydrogen flame propagation speed in ICEs in comparable operating conditions [16, 17, 32, 33]. The near-wall flame quenching is modelled through a y+-based variation of the turbulent flame speed, as firstly proposed in [34]. In particular, when the quenching distance exceeds the wall distance, the turbulent flame speed is reverted to the laminar one, to neglect the accelerating effect of turbulence on flame propagation. The quenching distance l_q is calculated as in Equation 2, where μ is the dynamic viscosity, ρ is the mixture density, k is the turbulent kinetic energy and c_μ is the turbulent model constant, which is set to 0.085.

Results and Discussion

The numerical results obtained through 3D CFD simulations are presented in this section and compared with the experimental measurements.

Concerning the cold phase of the engine, a very good agreement of the pressure profile for both operating conditions is obtained, as it can be seen in Figure 3, which shows the pumping loop of the lean operation (top) and the stoichiometric one (bottom). Consequently, the trapped mass at intake valve closing matches the experimental values in both cases. As for the flame development, while the lean case is characterized by a very good agreement with the experiments, a slight mismatch can be detected for the stoichiometric one. It is noteworthy to mention that the numerical results are obtained with the same setup concerning ignition and combustion.

Figure 4 shows the in-cylinder pressure, the apparent heat release rate traces during the combustion window and the combustion durations of the lean OC. An overall agreement is detected both in terms of pressure and apparent heat release trends. Particularly, the numerical pressure curve is almost superimposed to the experimental one both during the pressure-rise phase and the expansion stroke. A marginal underestimation of the peak pressure is noted, with the numerical value which is 2% lower than the experimental one. This behaviour is due to a slightly lower peak value of the heat release rate. This good agreement is also reflected in the combustion durations. For instance, both the MFB10-50 and MFB10-90 are well aligned with the experimental values, as the numerical results are respectively 9% and 1% slower.

As for the λ = 1 with a 40% EGR dilution operating condition, results are depicted in Figure 5. As it can be seen, concerning the in-cylinder pressure profile, a very good agreement can be detected up to the peak, whose value is overestimated by less than 1% of the experimental value. The mismatch detected on the

FIGURE 3 Experimental/numerical comparison of the pumping loop of the lean (top) and stoichiometric (bottom) cases.

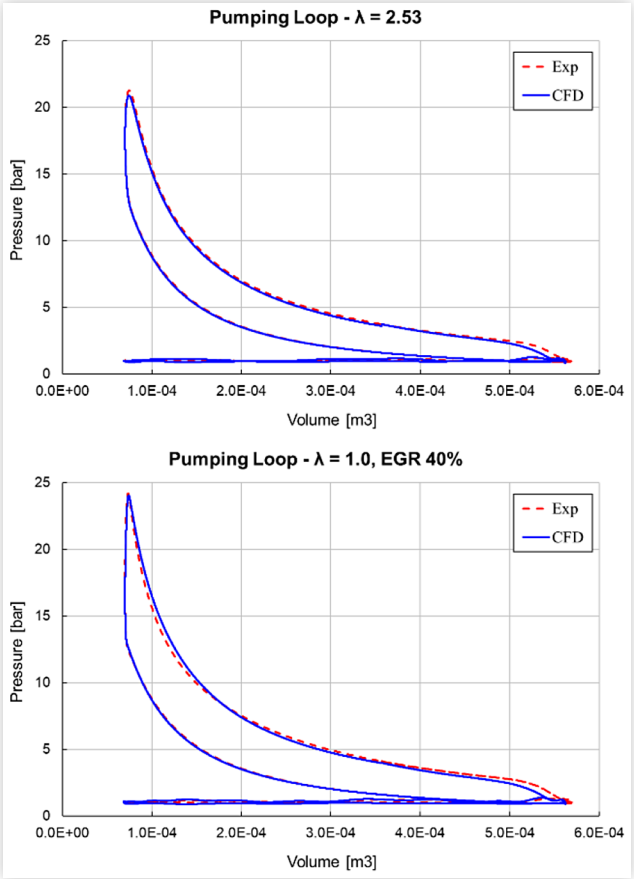

FIGURE 4 Experimental/numerical in-cylinder pressure, apparent heat release rate and combustion durations comparisons of the lean case.

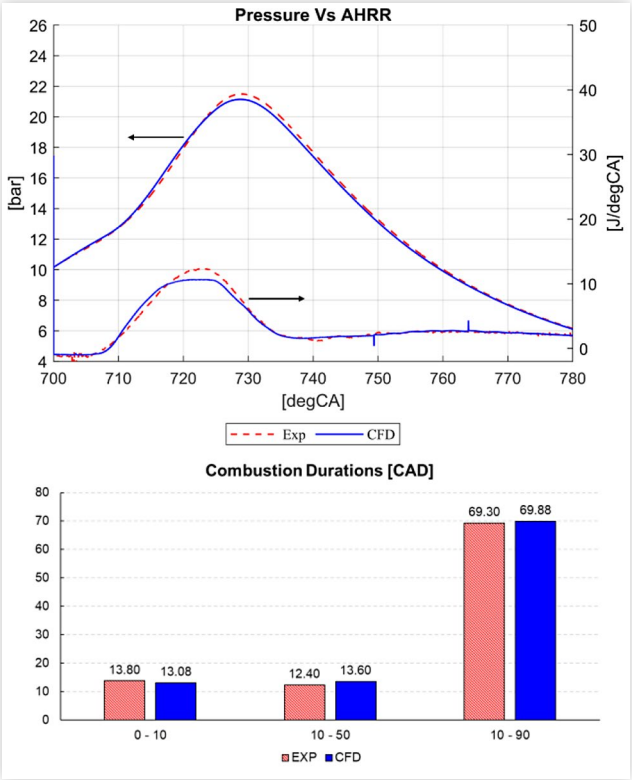

FIGURE 5 Experimental/numerical in-cylinder pressure, apparent heat release rate and combustion durations comparisons of stoichiometric cases.

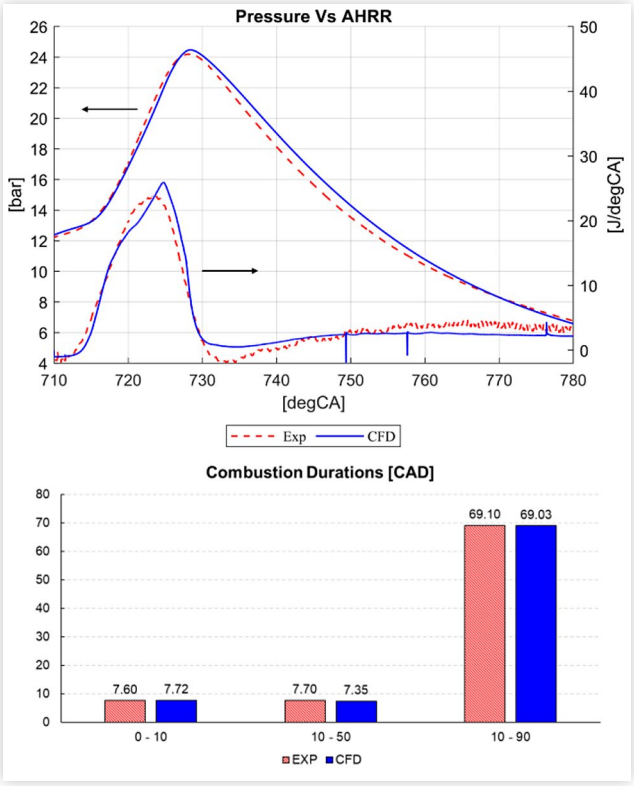

FIGURE 6 Error analysis of the studied cases.

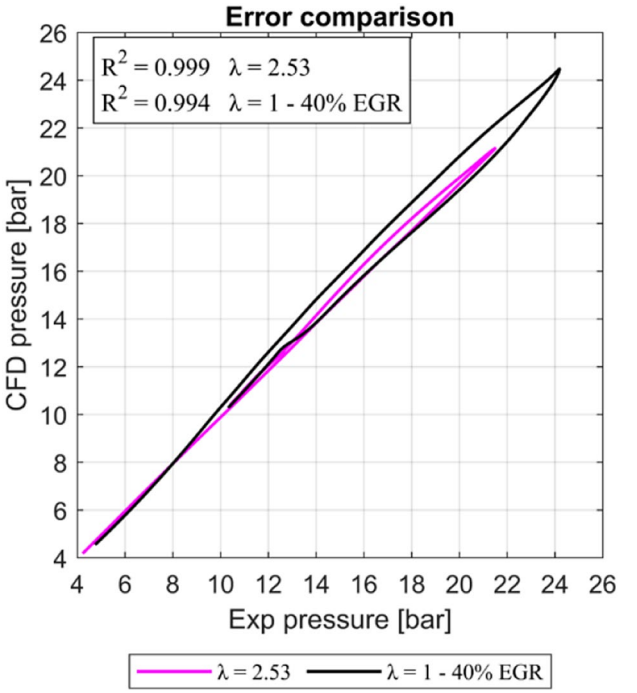

$$R^2 = 1 - \frac{\sum_{i=1}^{n} \left(y_i - \hat{y}_i\right)^2}{\sum_{i=1}^{n} \left(y_i - \bar{y}_i\right)^2} \quad (3)$$

pumping loop at the expansion stroke is here clearly visible, with an overestimation of the pressure in the combustion chamber from the pressure peak up to 50 CAD aTDC. However, the combustion durations are still well predicted by the used numerical setup, as the MFB10-50 from the simulation is 5% slower than the experimental value, while the MFB10-90 is superimposed to the testbench target.

Furthermore, it is worth noting that the ignition model setup adopted is able to well represent the experimental behaviour of the early stages of flame propagation. In fact, the mismatch noted with the experimental data concerning the MFB0-10 duration of both analysed cases is almost negligible: with the lean case a 5% faster flame development is detected, while with the stoichiometric and diluted mixture is 1% slower.

To quantify the difference between numerical and experimental profiles, the error analysis is carried out considering the coefficient of determination R^2, computed as reported in Equation 3, where y_i and $\hat{y}_i$ are the experimental and numerical pressure values the i-th sample, while $\bar{y}_i$ is the interval-average of the experimental pressure traces. The latter is calculated in the time-window between 700 and 800 CAD, which includes the combustion development and expansion phase of the piston. In Figure 6 the results are presented for the lean case (pink solid line) and the stoichiometric diluted one (black solid line).

As it can be seen, the in-cylinder pressure overestimation during the expansion stroke of the stoichiometric case is highlighted, with a maximum overestimation of 10% with respect to the experimental value. Conversely, for the lean case, the profile in Figure 6 is very close to the bisector of the plane, confirming the agreement between experiments and CFD.

In addition to the previous analysis, a mesh sensitivity is performed by halving the combustion chamber mesh size from 0.75 mm (identified as the medium mesh, MM) to 0.375 mm (identified as the fine mesh, FM) during the combustion phase. The results in terms of mean in-cylinder pressure and apparent heat release rate are depicted in Figure 7 (green solid line for FM, blue solid line for MM, red dashed line for the experimental traces).

Concerning the lean case, there are negligible differences between 715.0 CAD and 730.0 CAD, which identifies the combustion development time span, where the fine mesh leads to faster combustion, as it can be noted from the higher peak of heat release rate if related to the medium mesh results. This behaviour yields to a higher in-cylinder pressure peak, with an overestimation of 1% of the experimental value. The good agreement found between the two tested mesh setups can be also noted on the MFB trace reported in Figure 7 (middle). In particular, it can be seen that the results obtained with the fine mesh are superimposed to those with the medium mesh, leading to almost the same combustion durations. Indeed,

FIGURE 7 Mesh sensitivity analysis results on the lean case.

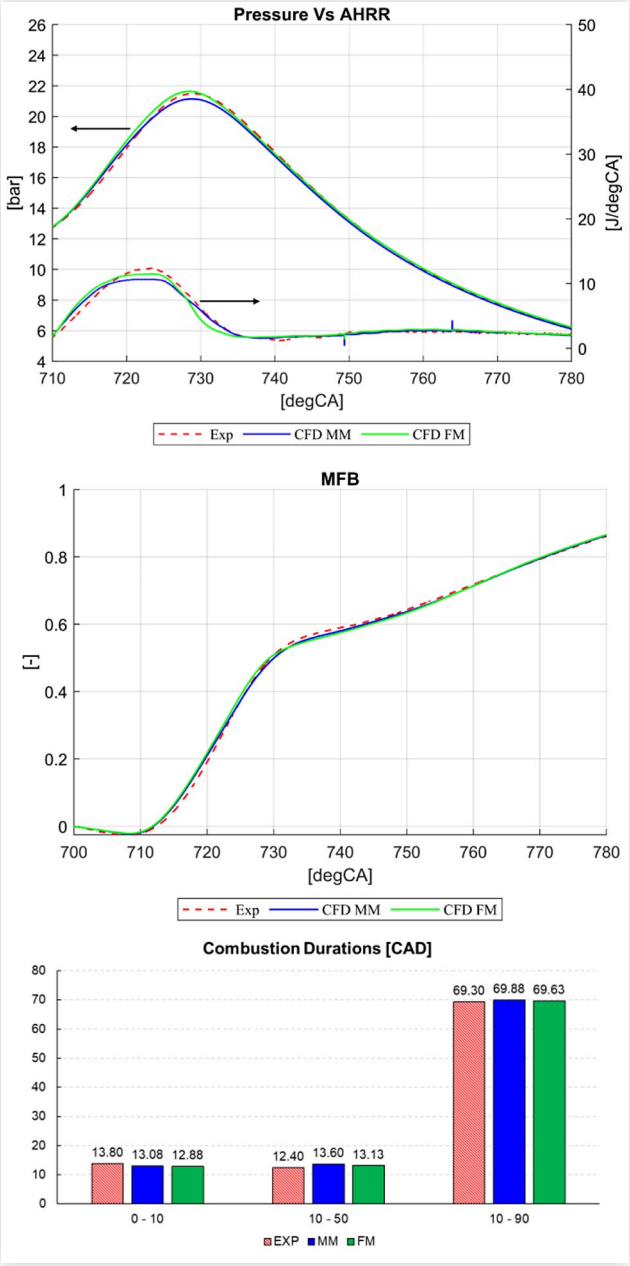

FIGURE 8 Mesh sensitivity analysis results on the stoichiometric case.

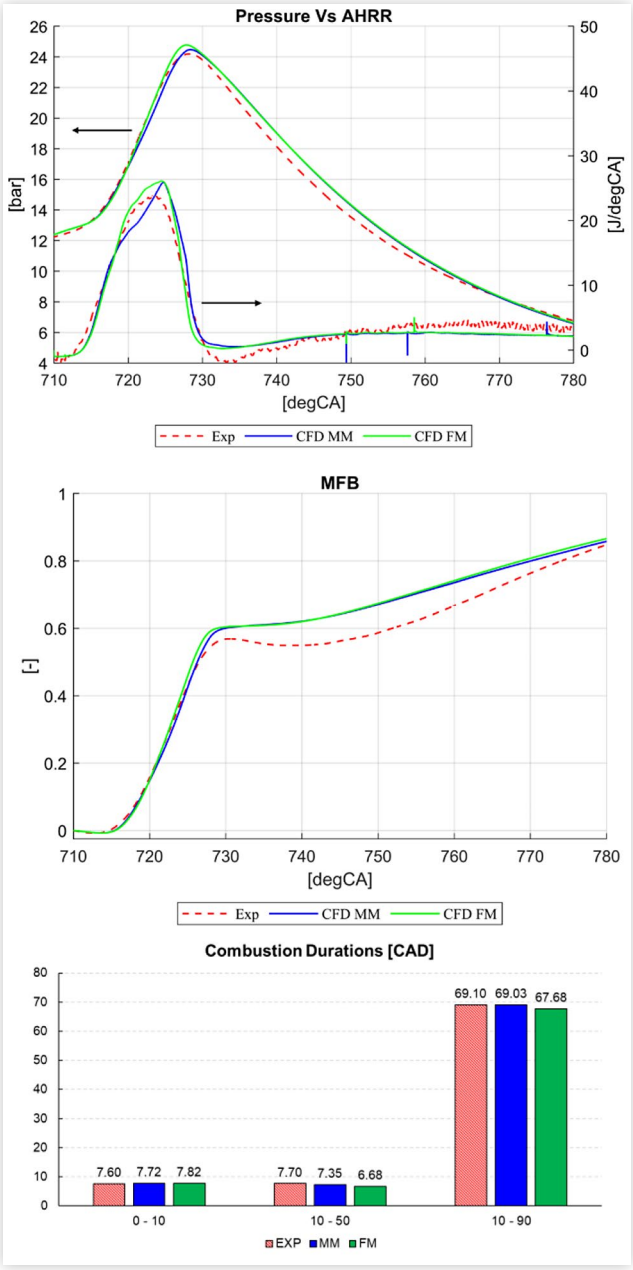

with the fine mesh the MFB10-90 duration is 0.25 faster than the one obtained with the medium mesh. Concerning the MFB profile, it is possible to note that with both mesh setups the slow heat release rate zone, which is visible after 730 CAD, is well captured. This portion of the combustion development refers to the time when the flame front approaches the liner and it slowly consumes the hydrogen trapped in the crevices between the piston and the cylinder liner.

As for the stoichiometric case, results are depicted in Figure 8. As it can be seen, a slight improvement in terms of heat release rate is observed. With the fine mesh, the experimental flame development is better matched, leading to a more accurate representation of the experimental heat release rate profile shape. The faster flame rate noted from 720 CAD to the heat release rate peak leads to a slight overestimation of the peak pressure in the combustion chamber, higher than the experimental one, and to an earlier MFB50 phasing if compared to the medium mesh result. This behaviour is confirmed by the combustion durations. As it can be seen from the histogram in Figure 8 (bottom), the combustion durations from MFB10 to MFB90, namely the turbulent combustion development, is 1.72 CAD shorter. As expected, it can also be noted that this sensitivity does not affect the early flame propagation stages, as the MFB0-10 duration obtained with the fine mesh is comparable to the result found with the medium mesh, as it is 0.04 CAD greater. It is also possible to note that even

with the fine mesh the overestimation of the pressure values during the expansion stroke is present. Therefore, the origin of the mismatch must be found in the reaction zone originating from the fuel trapped in the crevices, which in the CFD simulations seems to be faster than what can be seen experimentally. A deeper investigation of flame-wall interaction in the piston crevice region and its effect will be the object of future activities.

In terms of computational cost, the medium mesh consists of approximately 2.2 to 2.6 million cells from 700 CAD to 810 CAD, requiring around 4.5 hours of computation time using 104 cores. conversely, the total number of cells with fine mesh setup is approximately 3.0 to 6.0 million cells, with a computation time which is nearly double on equal number of cores. Considering the marginal gain in the solution and the delta computational cost of the simulations, the medium mesh setup is considered as the best trade-off.

Despite the two operating conditions yield to similar power output, different flame development rates can be noted, as it can be seen from the MFB10-50 experimental values (Figure 4 and Figure 5). In fact, the flame speed is found to be almost 40% faster with the stoichiometric and diluted mixture than with the lean one. The graph in Figure 9 shows the LFS (orange lines) and TFS (blue lines) average values calculated within the reaction zone for the λ = 2.53 (dashed lines) and λ=1.0 with 40% of EGR (solid lines).

As it can be noted, the TFS value in both cases tends asymptotically to the LFS value, as the turbulent kinetic energy decreases towards the walls. It is also noteworthy that after 728 CAD the TFS of the stoichiometric case becomes lower than the one computed one in the lean case. This behaviour is mainly related to the near-wall flame quenching model adopted in these simulations, which forces the TFS to the LFS value when the wall distance is lower than the quenching one. Indeed, at 728 CAD a wide portion of the flame front has approached the cylinder liner in the λ=1.0 case, while in the lean one most of the flame front is still developing in the quenching-free zone.

FIGURE 9 Laminar and turbulent flame speed comparison of the examined cases.

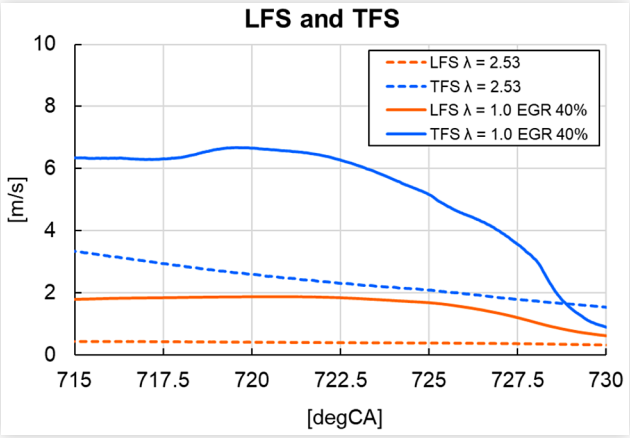

The combustion development of both operating conditions is plotted on the Borghi-Peters diagram. The turbulent fluctuation u', the laminar flame thickness δ_L and the integral length scale l_t are calculated respectively with Equation 4, 5 and 6, where k is the turbulent kinetic energy, α is the thermal conductivity of the mixture, ρ_u is the unburned gas density, C_p is the specific heat of the mixture, S_L is the laminar flame speed, c_μ is the turbulence model constant and ε is the turbulence dissipation rate.

As well known, the Borghi-Peters diagram is used to analyse the interplay between the reaction zone and the turbulent structures, from the integral scale to the Kolmogorov one. For instance, considering a turbulent flame regime, if both the aforementioned turbulent scales are slower than the chemistry, the inner structure of the reaction zone can be considered laminar, with an enhanced flame speed due to the wrinkling of the flame itself by the integral length scales (Flamelet Regime). By increasing turbulence, i.e. when the turbulent time scale of the Kolmogorov eddies becomes lower than the chemical time of the reaction, these structures are able to penetrate the reaction zone and thicken it (Thickened Regime). When also the integral scale becomes faster than chemistry, the reaction zone is distributed in all the domain (Well-Stirred Reactor). This diagram has been mainly designed to study the combustion regimes of carbon-based fuels (i.e. methane, gasoline, where the Lewis number Le ≈ 1). Therefore, it might not be suitable to identify the exact combustion regime of a hydrogen-fuelled engine. Nevertheless, it is able to give a good relative insight on the differences between the two investigated operating conditions, since the studied cases share the same engine revving speed, and therefore the almost equivalent turbulent characteristics at spark timing.

$$u' = \sqrt{\frac{2}{3} \cdot k} \tag{4}$$

$$\delta_L = \frac{2\alpha}{\rho_u C_p S_L} \tag{5}$$

$$l_t = c_\mu^{0.75} \cdot \frac{k^{2/3}}{\varepsilon} \tag{6}$$

In Figure 10, the results are displayed for the lean (green dotted line) and stoichiometric (pink dotted line) conditions. On these profiles, the main turbulent combustion development, namely from MFB10 to approximately MFB60, which identifies the instant when the flame starts to be quenched near the cylinder liner, is highlighted by the solid lines.

The results show that, despite the different mixture quality, both flame developments follow a similar path, as the morphology of the two traces is similar. This behaviour is expected given the homogeneity of the mixture, i.e. the laminar flame properties vary during the combustion process only because of the changes in pressure and unburnt temperature of the mixture, and given the similar

FIGURE 10 Borghi-Peters diagram of the analysed cases.

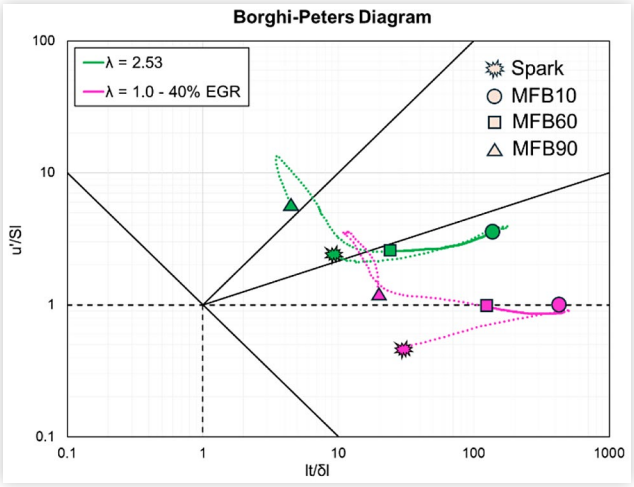

turbulent conditions at the beginning of the flame development. Therefore, the two profiles mainly differ because of the different raw values of the laminar flame speed and laminar flame thickness. Indeed, the case with λ=1.0 and 40% of EGR is characterized by a higher reactivity, and thus a higher flame speed and lower flame thickness. This behaviour can be clearly noted by comparing the early stages of flame development, from spark time to MFB10. In fact, given the very similar turbulence levels in both cases, and thus turbulent time scales, the shorter chemistry characteristic times of the stoichiometric mixture allow the process to fall entirely within the Wrinkled Flamelet Regime. On the contrary, the λ=2.53 case is characterized by a longer chemistry time scale, which is closer to the Kolmogorov time scale and therefore pushes the combustion closer to the Thickened Regime. Once the turbulent combustion sets in, the higher reactivity of the stoichiometric setup yields to a higher turbulence level, and thus the combustion regime gets closer to the corrugated flamelet one. As for the lean case, a marked increase of the turbulence level is not observed, and thus the combustion regime is similar to the one observed during the early stages of flame propagation. After MFB60, the reactivity of both mixtures decreases due to the expansion stroke. Therefore, the regimes for both mixtures move towards the Thickened Region due to the decreasing laminar flame speed. The last portion, where a decreasing x-component can be noted in both cases, can be attributed to the reaction zone approaching the piston crevice. Hence, the characteristic turbulent time scale that is exposed to the flame zone increases.

From this analysis it can be concluded that for the main combustion time window, where a major part of the pressure increase is located, the numerical setup adopted provides reliable results for both the tested operating conditions. To support this, a graphical visualization of the flame evolution is displayed in Figure 11 for both cases. Particularly, the progress variable equal to 0.5 isosurface is depicted, to graphically resemble the reaction zone. While for the λ=2.53 case the MFB60 is close to 740 CAD, for λ=1.0 with 40% of EGR it is close to 730 CAD. As it can be seen from Figure 11, at these two CA locations both flames are approaching the cylinder liner, and thus the majority of the turbulent combustion phase has taken place. From the sequences of images it is also possible to note the higher flame speed of the stoichiometric case, as the flame front covers the whole combustion chamber well before the lean case, despite having a delayed spark timing. This behaviour gives more time to the flame to reach the unburnt hydrogen trapped in the crevices, and it is favoured by the burning velocity predominance over the flow velocity, this last pushing the mixture out of the crevice.

Finally, the potential effect of thermo-diffusive instabilities on the flame speed is studied. It is well known that this phenomenon is non-negligible when considering hydrogen flames [35], particularly when the effective Lewis number of the mixture is lower than unity, which is typical of hydrogen lean mixtures [36]. Therefore, given their similar turbulence level, the two operating conditions considered in this study are suitable to understand the influence of the equivalence ratio on the hydrogen flame instability onset. Particularly, the methodology relies on the off-line calculation of the flame instability second order growth rate component ω_2, coherently with the one adopted by the authors in [16] which is based on the work of Fogla et al. [37]. Subsequently, the enhanced laminar flame speed is computed at the pressure and unburnt temperature values experienced in the combustion chamber during the combustion development. The results are presented in Figure 12, where the numerical pressure profiles are displayed with a colormap indicating the percentual increase of the laminar flame speed for the lean (left) and stoichiometric (right) cases. As it can be seen, while with the λ=1.0 with 40% of EGR case ω_2 is very close to zero, and thus the correction is negligible, a strong enhancement in terms of laminar flame speed is expected, with an average percentual increase of 98% throughout the combustion development and a peak value of +155%.

Despite this result seems to suggests that a relevant underestimation of the laminar flame speed might be introduced with the adopted numerical setup, it is important to note that the raw value throughout the flame development is lower than 0.4 m/s. Therefore, only a slightly faster flame speed is expected with the same turbulent flame speed setup.

Conclusions

In the present work, a numerical-experimental comparison on hydrogen combustion in an optically accessible ICE, using the well-known Darmstadt Engine. Two different mixture qualities, a lean undiluted and a stoichiometric with a high dilution percentage, are evaluated operating the engine at the same engine revving speed. The main outcomes can be briefly summarized below:

FIGURE 11 Temporal evolution of the flame front, identified through the iso-surface of 0.5 progress variable, for the studied cases

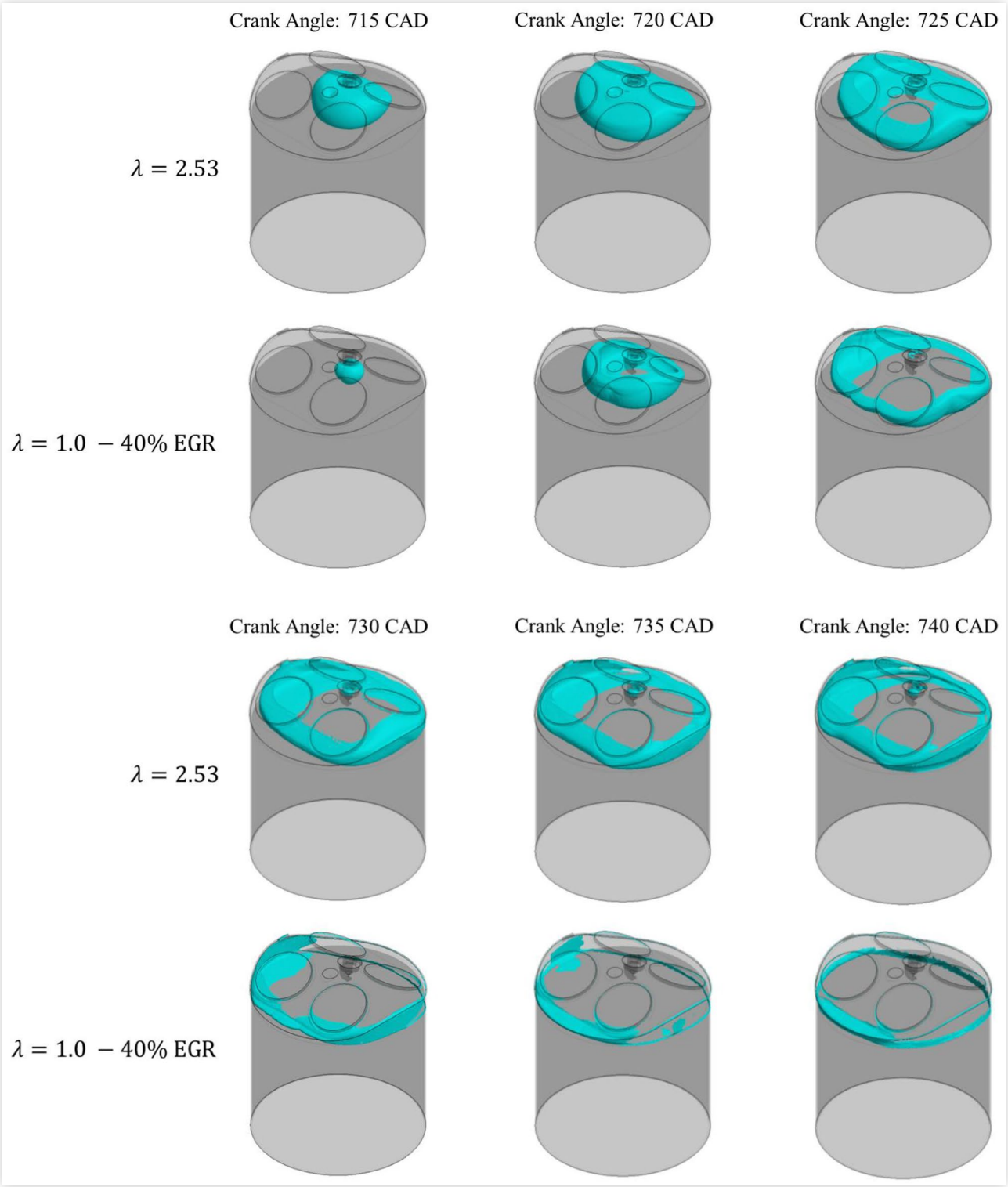

FIGURE 12 Laminar flame speed enhancement due to hydrogen thermo-diffusive instability on lean (left) and stoichiometric (right) cases.

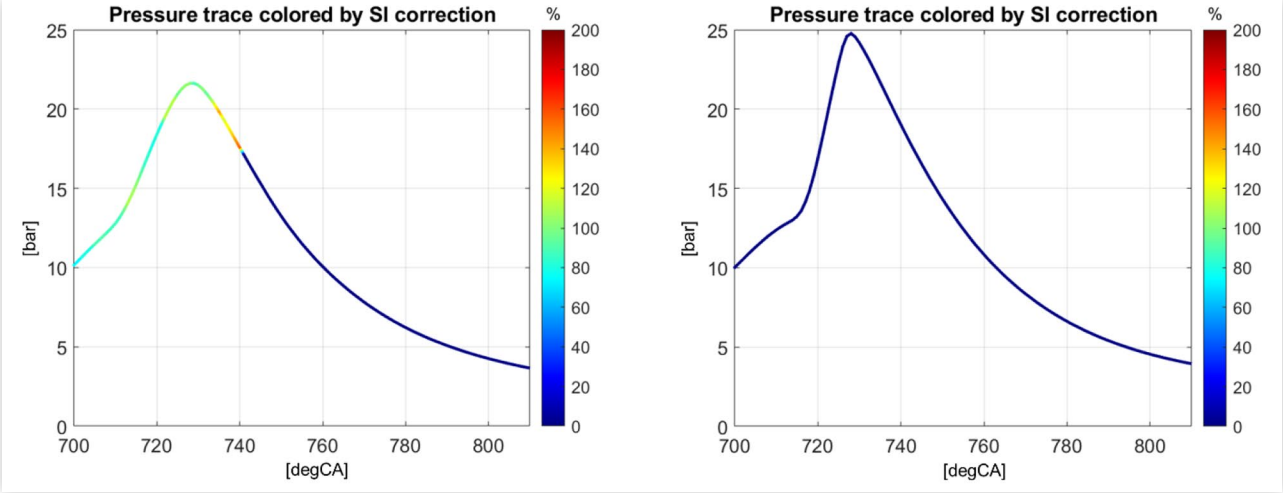

- The proposed numerical methodology is able to well reproduce the experimental acquisitions. Indeed, the numerical results present a similar pressure trace with respect to the experimental data in both conditions. A low overall R^2 factor is computed on the whole engine cycle, with a value less than 1%.
- The only noteworthy discrepancy found in the numerical-experimental comparison is the overestimation of the pressure value in the combustion chamber during the expansion stroke of the λ=1.0 with 40% of EGR case. This behaviour might be related to the overestimation of the flame development speed when it reaches the crevices between the cylinder liner and the piston. Further analyses on the near-wall flame interaction will be object of future activities.
- Given the very similar turbulent conditions of the two analysed operating conditions, the pathways of the flames on the Borghi-Peters diagram are similar. However, the different flame properties of the two mixtures yield to different combustion regimes, as almost all the combustion development falls inside the Flamelets Regimes with the stoichiometric mixture, while the lean one falls into the Thickened Flame and in the Well Stirred regions. Nevertheless, most of the turbulent combustion development falls within the Flamelets Region with both mixture qualities, and thus the numerical methodology presented here is deemed to be reliable.
- The offline analysis of the hydrogen flame instability second order component (ω_2) shows that the lean hydrogen operating condition can be affected by the thermo-diffusive instabilities, which are typical of a lower-than-unity Lewis number mixture. However, despite a strong correction of the laminar flame speed is predicted, the effect on the flame development speed is expected to of secondary importance, given the low laminar flame speed absolute value throughout the turbulent combustion development. Further analyses incorporating the online solution of the flame speed enhancement due to ω_2 will be the object of future work.
- Future activities may also include a numerical investigation with experimental validation of NO_x emissions, in order to obtain a more general understanding of the best mixture strategies to be adopted when considering a hydrogen-fuelled internal combustion engine.

References

1. Eisele, K., "Fit for 55 package: Recasting the Energy Efficiency Directive," December 2021, https://www.europarl.europa.eu/RegData/etudes/BRIE/2021/699462/EPRS_BRI(2021)699462_EN.pdf.
2. Sharma, S. and Ghoshal, S.K., "Hydrogen the Future Transportation Fuel: From Production to Applications," *Renewable and Sustainable Energy Reviews* 43 (2015): 1151-1158, doi:10.1016/j.rser.2014.11.093.
3. Lee, S., Kim, K., Lee, J., Kim, Y. et al., "NOx Reduction in Hydrogen-Fueled Direct-Injected Spark Ignition (DISI) Engine Using Post-Injection Strategy: Experimental and Chemical Kinetics Approaches," *Energy* 324 (2025): 136085, doi:10.1016/j.energy.2025.136085.
4. Qin, Z., Zhang, H., Liu, F., Wang, X. et al., "A Coupled Study of Injection Strategy on Gas Motion and Heat Transfer in a Diesel Ignition Linear Hydrogen Engine," *International Journal of Hydrogen Energy* 82 (2024): 502-512, doi:10.1016/j.ijhydene.2024.07.444.
5. Liu, X., Yang, L., Chan, Q.N., and Kook, S., "Split Injection Strategies for a High-Pressure Hydrogen Direct Injection in a Small-Bore Dual-Fuel Diesel Engine," *International Journal of Hydrogen Energy* 57 (2024): 904-917, doi:10.1016/j.ijhydene.2024.01.065.

6. Qin, Z., Liu, F., Zhang, H., Wang, X. et al., "Study of Hydrogen Injection Strategy on Fuel Mixing Characteristics of a Free-Piston Engine," *Case Studies in Thermal Engineering* 56 (2024), doi:10.1016/j.csite.2024.104279.
7. Purayil, S.T.P., Hamdan, M.O., Al-Omari, S.A.B. et al., "Impact of Intake Air Pressure and Temperature on Performance and Hydrogen Knock Limit in a Spark-Ignition Engine Using Hydrogen-Gasoline Blends," *Applied Thermal Engineering* 263 (2025), doi:10.1016/j.applthermaleng.2024.125331.
8. Madia, M., Vaccari, M., Dalseno, L., Cicalese, G. et al., "Assessment of Knock Tendency in a Hydrogen-Fuelled High-Performance Internal Combustion Engine: A Chemistry-Based Numerical Study," SAE Technical Paper 2025-01-8429 (2025), doi:10.4271/2025-01-8429.
9. Park, H., Lee, J., Oh, S., Kim, C. et al., "Strategies of Hydrogen-Air Mixture Formation for Suppressing Backfire, Pre-ignition, and Knock in Full-Load Operations of Hydrogen Heavy-Duty Engines," *Energy* (2025), doi:10.1016/j.energy.2025.136343.
10. Mortimer, J., Poursadegh, F., Brear, M., Yoannidis, S. et al., "Extending the Knock Limits of Hydrogen DI ICE Using Water Injection," *Fuel* 335 (2023), doi:/10.1016/j.fuel.2022.126652.
11. Navale, S.J., Kulkarni, R.R., and Thipse, S.S., "An Experimental Study on Performance, Emission and Combustion Parameters of Hydrogen Fueled Spark Ignition Engine with the Timed Manifold Injection System," *Int J Hydrogen Energy* 42, no. 12 (2017): 8299-8309, doi:10.1016/j.ijhydene.2017.01.059.
12. Schefer R.W., White, C. and Keller J., "Chapter 8 – Lean Hydrogen Combustion," in: *Lean Combustion* (pp. 213-254), 2008, 10.1016/B978-012370619-5.50009-1
13. Turner, J.W.G., Verhelst, S., and Marquez, M.E., "The Potential of Hydrogen Internal Combustion Engines for Heavy-Duty Applications," *The Clean Hydrogen Economy and Saudi Arabia* (2024): 606-637, doi:10.4324/9781003294290-26.
14. Verhelst, S. and Wallner, T., "Hydrogen-Fueled Internal Combustion Engines," *Prog .Energy Combust Sci* 35, no. 6 (2009): 490-527, doi:10.1016/j. pecs.2009.08.001.
15. Rakopoulos, C.D., Kosmadakis, G.M., and Pariotis, E.G., "Evaluation of a Combustion Model for the Simulation of Hydrogen Spark-Ignition Engines Using a CFD Code," *International Journal of Hydrogen Energy* 35, no. 22 (2010): 12545-12560, doi:10.1016/j.ijhydene.2010.09.002.
16. Sfriso, S., Berni, F., Breda, S., Fontanesi, S. et al., "Proposal and Validation of 3D-CFD Framework for Ultra-Lean Hydrogen Combustion in ICEs," SAE Technical Paper 2024-01-2685 (2024), doi:10.4271/2024-01-2685.
17. Sfriso, S., Berni, F., Fontanesi, S., d'Adamo, A. et al., "Combination of G-Equation and Detailed Chemistry: An Application to 3D-CFD Hydrogen Combustion Simulations to predict NOx Emissions in Reciprocating Internal Combustion," *Int J Hydrogen Energy* 89 (2024): 161-176, doi:10.1016/j.ijhydene.2024.09.252.
18. Dhyani, V. and Subramanian, K.A., "Fundamental Characterization of Backfire in a Hydrogen Fuelled Spark Ignition Engine Using CFD and Experiments," *International Journal of Hydrogen Energy* 44, no. 60 (2019): 32254-32270, doi:10.1016/j.ijhydene.2019.10.077.
19. Iacovano, C., Berni, F., Barbato, A., and Fontanesi, S., "A Preliminary 1D-3D Analysis of the Darmstadt Research Engine under Motored Condition," *E3S Web Of Conferences* 197 (2020): 1-12, doi:10.1051/e3sconf/202019706006.
20. Raj, A.G.S. and Mishra, C.S., "Simulation and Experimental Data Resemblance of Darmstadt Spark Ignition Engine with Different Turbulence Models – A Computational Fluid Dynamics Cold Flow Data," *Data in Brief* 43, doi:10.1016/j.dib.2022.108340.
21. Barbato, A., Fontanesi, S., and d'Adamo, A., "Impact of Grid Density and Turbulence Model on the Simulation of In-Cylinder Turbulent Flow Structures - Application to the Darmstadt Engine," SAE Technical Paper 2021-01-0415 (2021), doi:10.4271/2021-01-0415.
22. Baum, E., Peterson, B., Böhm, B., and Dreizler, A., "On the Validation of LES Applied to Internal Combustion Engine Flows: Part 1: Comprehensive Experimental Database," *Flow Turbul. Combust.* (2014), doi:10.1007/s10494- 013-9468-6.
23. Welch, C., Illmann, L., Schmidt, M. et al., "Experimental Characterization of the Turbulent Intake Jet in an Engine Flow Bench," *Exp Fluids* 64 (2023), doi:10.1007/s00348-023-03640-9.
24. Yakhot, V. and Orszag, S.A., "Renormalization Group Analysis of Turbulence. I. Basic Theory," *Journal of Scientific Computing* 1, no. 1 (1986): 3-51, doi:10.1007/BF01061452.
25. Berni, F., Cicalese, G., Borghi, M., and Fontanesi, S., "Towards Grid-Independent 3D-CFD Wall-Function-Based Heat Transfer Models for Complex Industrial Flows with Focus on In-Cylinder Simulations," *Appl Therm Eng.* 190 (2021), doi:10.1016/j.applthermaleng.2021.116838.
26. Berni, F., Cicalese, G., Sparacino, S., and Cantore, G., "On the existence of universal wall functions in in-cylinder simulations using a low-Reynolds RANS turbulence model," *AIP Conference Proceedings* 2191 (2019), doi:10.1063/1.5138752.
27. Berni, F. and Fontanesi, S., "A 3D-CFD Methodology to Investigate Boundary Layers and Assess the Applicability of Wall Functions in Actual Industrial Problems: A Focus on In-Cylinder Simulations," *Appl Therm Eng* 174 (2020), doi:10.1016/j.applthermaleng.2020.115320.
28. Colin, O. and Truffin, K., "A Spark Ignition Model for Large Eddy Simulation Based on an FSD Transport Equation (ISSIM-LES)," *Proceedings of the Combustion Institute* 33, no. 2 (2010): 3097-3104, doi:10.1016/j.proci.2010.07.023.
29. Duclos, J.-M. and Colin, O., "(2-25) Arc and Kernel Tracking Ignition Model for 3D Spark-Ignition Engine Calculations((SI-7)S. I. Engine Combustion 7-Modeling)," in *The International Symposium on Diagnostics and Modeling of Combustion in Internal Combustion Engines*, 46, 2001, 10.1299/jmsesdm.01.204.46
30. Verhelst, S., T'Joen, C., Vancoillie, J., and Demuynck, J., "A Correlation for the Laminar Burning Velocity for Use

in Hydrogen Spark Ignition Engine Simulation," *International Journal of Hydrogen Energy* 36, no. 1 (2011): 957-974, doi:10.1016/j.ijhydene.2010.10.020.

31. Konnov, A.A., "Yet Another Kinetic Mechanism for Hydrogen Combustion," *Combustion and Flame* 203 (2019): 14-22, doi:10.1016/j.combustflame.2019.01.032.
32. Sfriso, S., Berni, F., Fontanesi, S., Breda, S. et al., "Proposal and Validation of a Numerical Framework for 3D-CFD In-Cylinder Simulations of Hydrogen Spark-Ignition Internal Combustion Engines," *Int J Hydrogen Energy* 53 (2024): 114-130, doi:10.1016/j.ijhydene.2023.12.027.
33. Ramalho Leite, C., Brequigny, P., Borée, J., and Foucher, F., "Early Flame Development Characterization of Ultra-Lean Hydrogen–Air Flames in an Optical Spark-Ignition Engine," *Proceedings of the Combustion Institute* 40, no. 1–4 (2024), doi:10.1016/j.proci.2024.105260.
34. Bruneaux, G., Poinsot, T., and Ferziger, J.H., "Premixed Flame–Wall Interaction in a Turbulent Channel Flow: Budget for the Flame Surface Density Evolution Equation and Modelling," *Journal of Fluid Mechanics* 349: 191-219, doi:10.1017/S0022112097006769.
35. Mitani, T. and Williams, F.A., "Studies of Cellular Flames in Hydrogen-Oxygen-Nitrogen Mixtures," *Combustion and Flame* 39, no. 2 (1980): 169-190, doi:10.1016/0010-2180(80)90015-2.
36. Berger, L., Attili, A., and Pitsch, H., "Intrinsic Instabilities in Premixed Hydrogen Flames: Parametric Variation of Pressure, Equivalence Ratio, and Temperature. Part 2 – Non-Linear Regime and Flame Speed Enhancement," *Combustion and Flame* 240 (2022), doi:10.1016/j.combustflame.2021.111936.
37. Fogla, N., Creta, F., and Matalon, M., "Effect of Folds and Pockets on the Topology and Propagation of Premixed Turbulent Flames," *Combust Flame* 162, no. 7 (2015): 2758-2777, doi:10.1016/j.combustflame.2015.04.012.

Contact Information

Manuel Madia
Internal Combustion Engine Research Group
University of Modena and Reggio Emilia
manuel.madia@unimore.it

Sebastiano Breda, PhD
Internal Combustion Engine Research Group
University of Modena and Reggio Emilia
sebastiano.breda@unimore.it

Acknowledgements

The experimental work described in this paper has been conducted by Benjamin Böhm and Pedro Ye from the Technical University of Darmstadt.

Support by Deutsche Forschungsgemeinschaft through FOR 2687 "Cyclic variations in highly optimized hydrogen-fueled spark-ignition engines: experiment and simulation of a multi-scale causal chain"—project number 423224402—is kindly acknowledged.

The numerical analyses were financed by European Union-Next generation EU through the "PIANO NAZIONALE DI RIPRESA E RESILIENZA (PNRR) – MISSIONE 4 COMPONENTE 2, "Dalla ricerca all'impresa" INVESTIMENTO 1.4, (CN00000023). In the context of the "Sustainable Mobility Center (Centro Nazionale per la Mobilità sostenibile – CNMS)" – Spoke 12 – Avviso MUR 3138/2021 modificato con DD 3175/2021.

ISSN 0148-7191